JOURNAL OF GEOPHYSICAL RESEARCH, VOL. 106, NO. A11, PAGES 25,673–25,681, NOVEMBER 1, 2001

Observations and modeling of neutral gas releases from the APEX satellite

E. Y. Choueiri
Electric Propulsion and Plasma Dynamics Laboratory, Princeton University, Princeton, New Jersey, USA

V. N. Oraevsky, V. S. Dokukin, A. S. Volokitin, S. A. Pulinets, and Y. Y. Ruzhin
Institute of Terrestrial Magnetism, Ionosphere and Radio Wave Propagation (IZMIRAN), Troitsk, Russia

V. V. Afonin
Space Research Institute, Moscow, Russia

Abstract. Results from experiments of neutral xenon gas releases in the ionosphere are presented. The releases were made from the scientific satellite APEX, which had various plasma and field diagnostics. An enhancement of HF wave activity over a broad band (0.1–10 MHz) is shown to occur during releases made in the sunlight at high pitch angles to the magnetic field. No changes of plasma density were detected, but electron temperature measurements indicate electron energy enhancements during the releases. Theoretical calculations based on the conditions of the APEX releases show that charge-exchange collisions and elastic scattering of the injected Xe neutrals by the ambient plasma can lead to an ion beam instability that may account for the observed wave and electron energy enhancements. The interaction is akin to the critical ionization velocity effect. We calculate that because of the low injection density, this turbulence-fueled ionization should have a low yield ($<1\%$), which may explain the lack of detectable plasma density enhancement.

1. Introduction

Neutral gas releases in the ionosphere have been used to study various natural and artificially staged plasma interactions and, in particular, to investigate a fundamental plasma physics effect known as the critical ionization velocity (CIV). The CIV effect was first postulated by *Alfvén* [1954], who hypothesized that a neutral gas streaming through a plasma in a magnetic field will suddenly become ionized when the relative velocity between the neutral gas and the plasma reaches or exceeds a critical value,

$$v_{ci} = \left(\frac{2\varepsilon_i}{M}\right)^{1/2}, \tag{1}$$

where M is the atomic mass of the neutral atom and ε_i is its ionization potential.

The CIV effect has been recognized as an instability-driven ionization process that is central to many problems in plasma dynamics. It has been first invoked in the context of cometary physics, the formation of the solar system, planetary tori, and more practically in the interaction of spacecraft exhaust with plasma environment, ionization processes in plasma guns and plasma thrusters. Reviews of the effect and its manifestations are given by *Brenning* [1992] and *Biasca* [1992].

The importance of the Earth ionosphere and magnetosphere as an ideal laboratory to test the CIV phenomenon has been widely recognized [*Mobius et al*., 1979]. The relative velocity between a neutral gas injected from a rocket or spacecraft and the background plasma is effectively the orbital velocity, which is larger than u_{ci} for a few gases and alkali vapors (e.g., Xe, Kr, Cs, Ba, and Sr).

Most of the previous gas releases studied in the context of CIV were shaped-charge releases of alkali metals in the ionosphere from sounding rockets [*Haerendel*, 1982; *Haerendel et al*., 1986; *Torbert*, 1990; *Swenson et al*., 1990; *Swenson et al*., 1991]. A critical review of these experiments [*Torbert*, 1990] has indicated that no single experiment has yet produced simultaneously the high ionization yield, wave activity, and evidence of high-energy electrons that are expected to occur in an ideal CIV interaction.

The use of orbiting spacecraft for gas release studies generally offers an advantage over rocket experiments, as it allows for parametric and repetitive tests with more plasma diagnostics. The use of xenon for shuttle-based CIV studies takes advantage of the fact that the shuttle orbital velocity of 7 km s^{-1} exceeds the 4.2 km s^{-1} critical ionization velocity for xenon. One such experiment from the space shuttle was ATLAS 1 [*Burch et al*., 1994], which was designed to optimize the conditions for a strong yield. A factor of 60 increase in plasma density was observed [*Marshall et al*., 1993] along with optical emission and enhanced wave activity in the lower hybrid range [*Choueiri et al*., 1994]. Numerical simulation of that experiment showed that a CIV-type interaction was a likely explanation for the recorded effects [*Okuda and Choueiri*, 1994].

APEX (Active Plasma Experiment in Space) is a scientific satellite (Intercosmos 25) of the Institute of Terrestrial Magnetism Ionosphere and Radio Wave Propagation (IZMIRAN), in Russia. The APEX satellite was launched on December 18, 1992, and placed in a polar orbit with an altitude ranging between 400 and 3000 km. APEX included an extensive battery

Paper number 2001JA000040.
0148-0227/01/2001JA000040$09.00

Table 1. Orbital Conditions for the APEX Neutral Gas Releases Whose HF Wideband Data Are Discussed in This Paper

Orbit	Date, GMT	Altitude, km	Latitude/Longitude	Velocity, km s^{-1}	Pitch	Sun/Shade
419	Jan. 22, 1992, 1157:30	666.4	59.54°N/−17.75°W	8.01	95°–113°	sun
490	Jan. 28, 1992, 1157:00	838.7	58.91°N/−8.8°W	7.84	95°–113°	sun
426	Jan. 23, 1992, 0151:20	573.1	46.02°N/−8.898°W	8.1	64°–71°	shade
496	Jan. 28, 1992, 2347:28	522.6	40.31°N/−29.3°W	8.15	57°–70°	shade

of plasma diagnostics and a Hall plasma thruster, which was not used for propulsion but rather served as a xenon plasma source for active experiments. The operation of this device in a no-discharge mode provided the opportunity to study the effects of neutral xenon gas releases. Since these releases were not planned when the satellite hardware was designed, they were not actively optimized to maximize the ionization yield in a CIV-type interaction. Indeed, it is important to note that the mass flow rate of xenon on APEX was only 5 mg s^{-1}, in contrast with 131 g s^{-1} on ATLAS 1. However, unlike the 100 ms pulsed gas injections of ATLAS 1, the APEX releases lasted for a few minutes each and provided different conditions in which to study the interaction.

In this paper we present wave and plasma measurements made during these gas releases and provide an interpretation of some of the observed effects using theoretical calculations based on the measured parameters. In section 2 we describe the scientific hardware and diagnostics used during the releases. The experimental data are presented and discussed in section 3. In particular, we look at the HF waves, plasma density, and electron temperature along and perpendicular to the geomagnetic field, recorded during the releases. In section 4 we present a theoretical description of these releases including models for the several processes that may contribute to the formation of ion seeds, the resulting nonequilibrium distribution of ions, the quasi-linear theory of instability of the ion beam confined spatially by a background plasma, the heating of electrons in this process, and the resulting ionization. Calculations using the theory with the measured parameters of the APEX releases are used to provide possible explanations for some of the observed effects.

2. APEX Hardware and Diagnostics

The suite of scientific instruments on board APEX included a xenon plasma source (Hall thruster) called SPT-100 (operated in a no-discharge mode during the neutral gas releases) and plasma particle and field diagnostics that allow measurements of microparameters and macroparameters including thermal and suprathermal components of the plasma, dc component of the magnetic and electrical fields, and electromagnetic fields in the ULF/ELF/VLF/HF ranges of frequencies.

For a number of technical and logistic reasons, not all the instruments were functioning during the neutral gas releases reported here. Consequently, no data on electron and ion energy distributions or low-frequency components of the electric and magnetic fields are presently available. In particular, no wave measurements in the lower hybrid range are available. A high-frequency antenna, receiver, and spectrum analyzer allowed measurements of one component of fluctuating electrical and magnetic fields in a range of frequencies between 0.1 and 10 MHz. This HF module was the source of all the wave data shown in this paper.

The plasma parameters (density of ions and three components of temperature of electrons) were measured by a device called KM-10, which uses 3.5 cm diameter flat nickel electrical probes. One probe was allocated for the continuous control of probe potential relative to the body of the satellite. Because of the high input impedance of the differential amplifier, the potential of the probe was close to the potential determined by a balance between the electron and ongoing ion flows. The KM-10 is capable of measuring a difference of potentials down to ±90 V. The detector part of the KM-10 device was fixed on a beam of length 1 m in front of the solar panels in the ram direction.

The dc magnetic field is measured with a three-axis fluxgate magnetometer with a dynamic range of ±6400 nT. Data from another three-axis service magnetometer, which is part of the attitude control system, were also available as part of the scientific telemetry stream.

As already mentioned, the neutral xenon gas releases were made through a Hall plasma thruster operating in a no-discharge mode. The thruster's axis of symmetry is at 45° with respect to the satellite vertical axis. The mass flow rate was about 5 mg s^{-1} and lasted for periods of 3–7 min.

3. Experimental Observations

The relevant orbital conditions for some of the APEX neutral gas releases are shown in Table 1. In this paper we discuss data from orbits 419, 490, 426, and 496, which represent typical experiments. The first two correspond to releases done at high pitch angles and in sunlight, while in the last two the releases were made at relatively low pitch angles and in darkness.

It is important to note that all the high–pitch angle releases that we studied were done in sunlight while all the low–pitch angle releases were done in darkness. This is due to an unplanned synchronicity between the attitude dynamics along the polar orbit, the solar illumination cycle, and the timing of the releases.

3.1. Broadband High-Frequency Emission

The most pronounced manifestation of the effects of the neutral gas releases occurred in the HF wave activity recorded during the high–pitch angle injections.

The features of the observed phenomenon can be summarized as follows:

All the studied neutral xenon releases with large (near normal) pitch angles, namely, between 85° and 115°, excited some high-frequency waves in the range 3–10 MHz (no data above 10 MHz are available).

All the studied neutral xenon releases with relatively small (i.e., oblique) pitch angles, namely, between 57° and 71°, did not result in any such wave emission.

These observations are supported by the following HF wide-

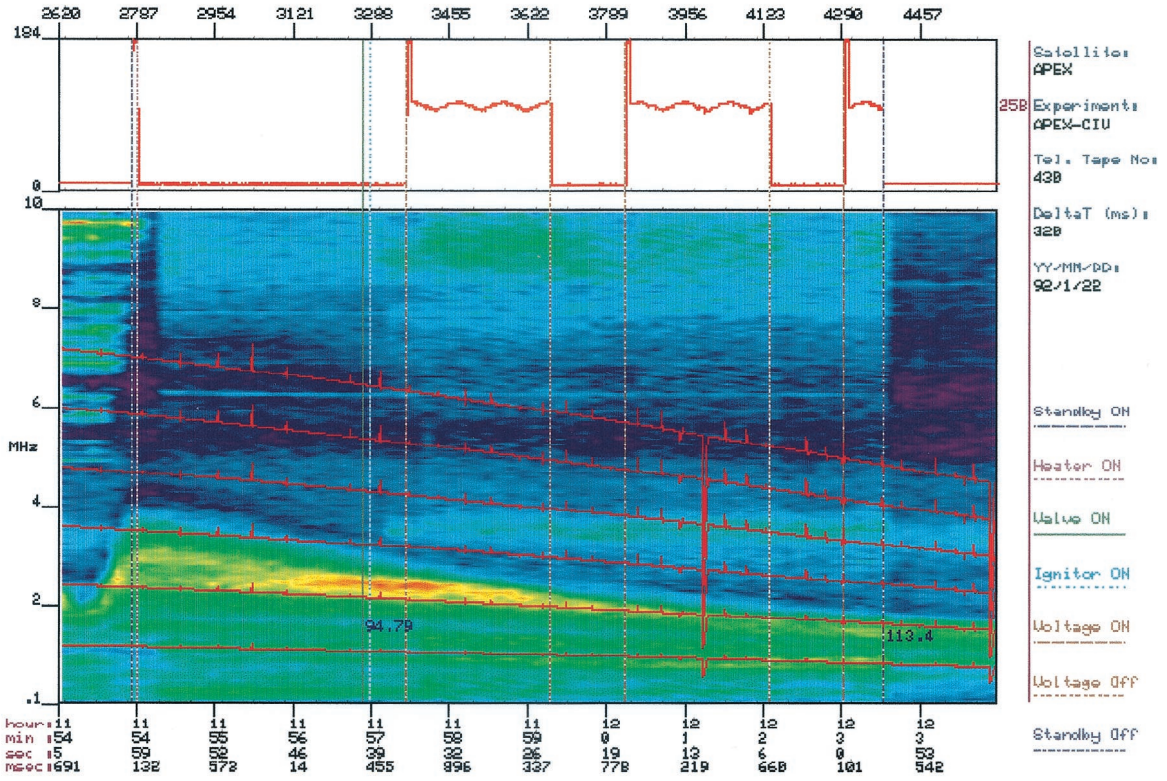

Plate 1. High–pitch angle release. Wideband HF data in the range 0.1–10 MHz for a neutral xenon release conducted during orbit number 419.

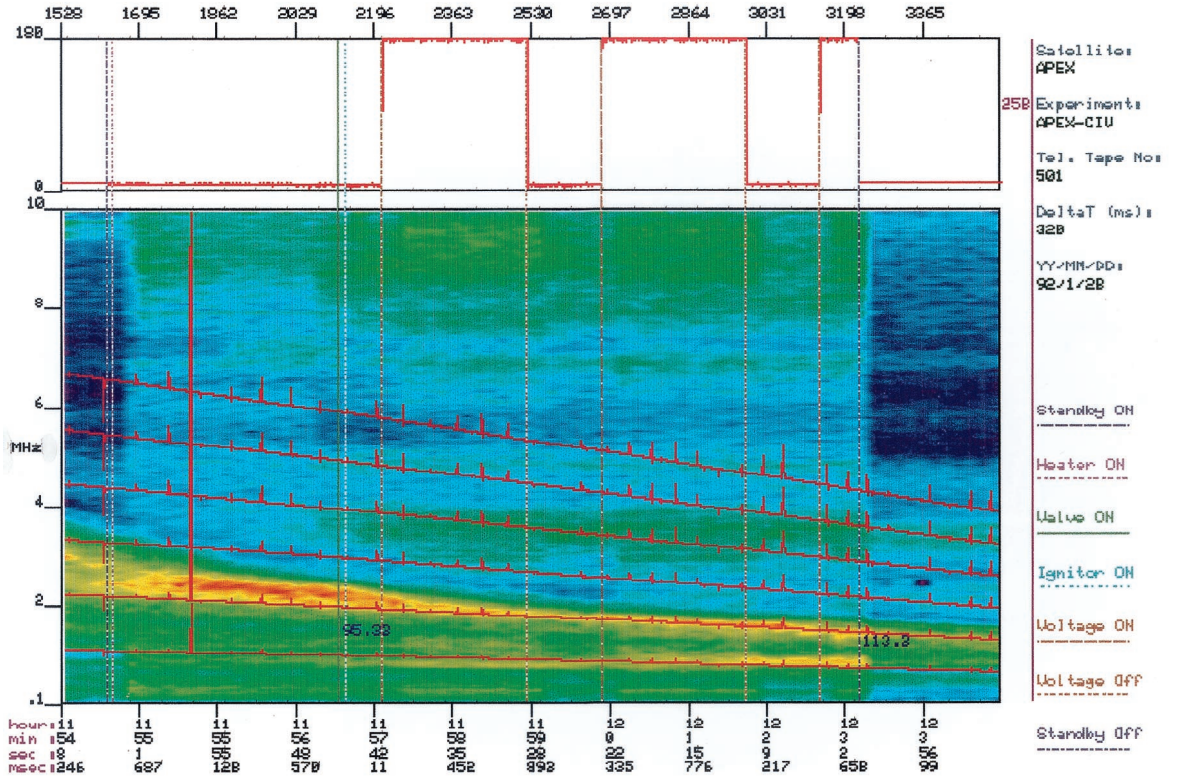

Plate 2. High–pitch angle release. Wideband HF data for orbit number 490. Same nomenclature as in Plate 1. Pitch angle varies from 95° to 113°.

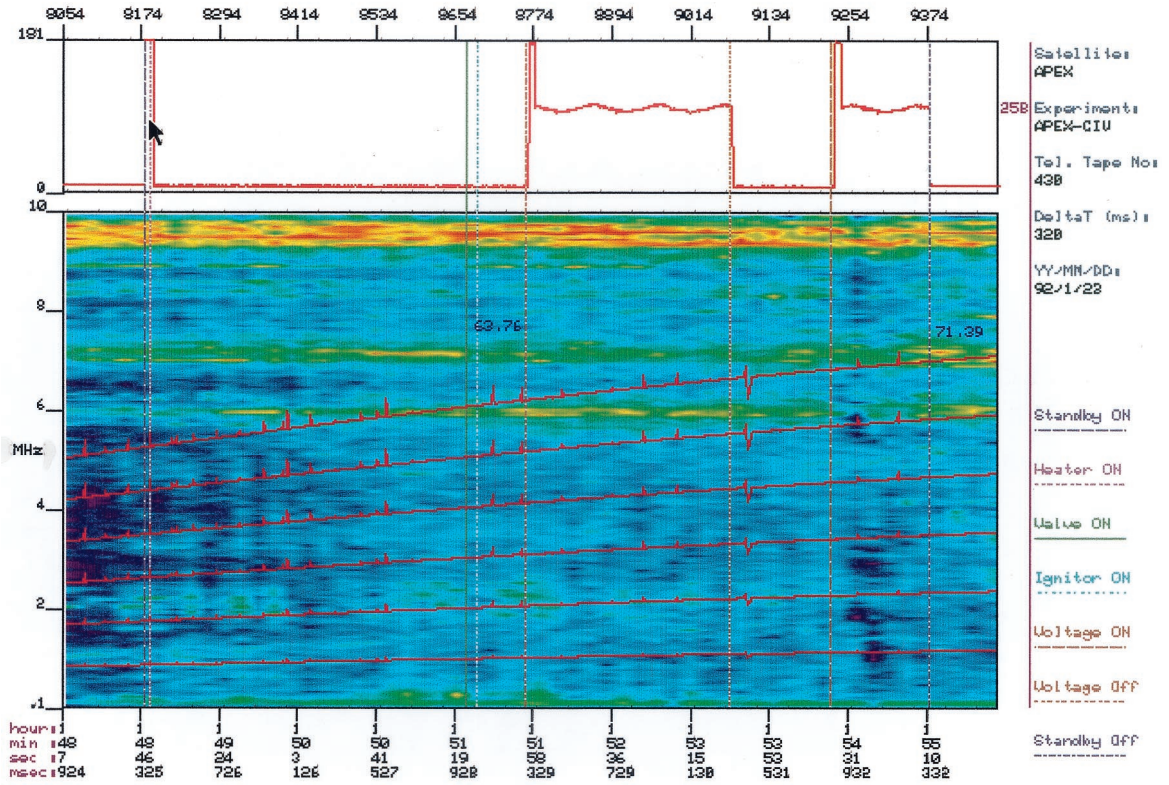

Plate 3. Low–pitch angle release. Wideband HF data for orbit number 426. Same nomenclature as in Plate 1. Pitch angle varies from 64° to 71°.

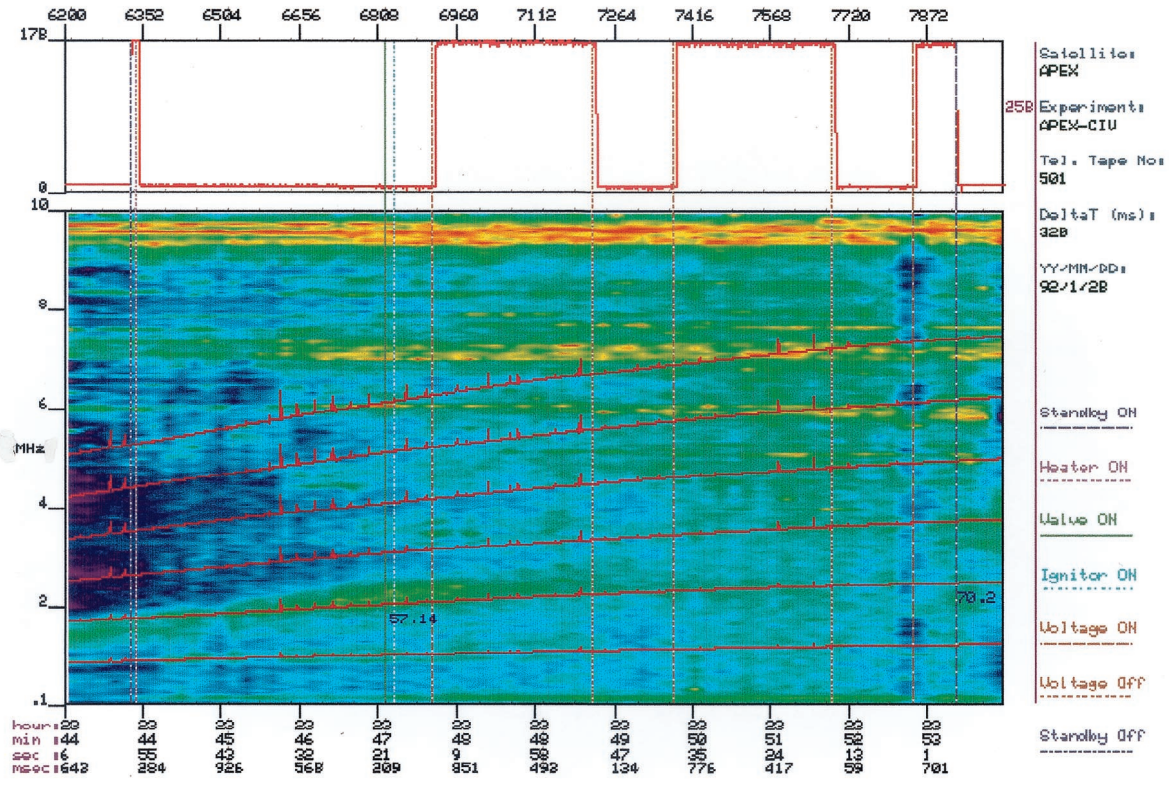

Plate 4. Low–pitch angle release. Wideband HF data for orbit number 496. Same nomenclature as in Plate 1. Pitch angle varies from 57° to 70°.

band data, which represent two typical high–pitch angle releases and two low–pitch angle releases.

In Plate 1 we show typical HF wideband data in the range 0.1–10 MHz for a neutral xenon release conducted during orbit number 419. The log of the amplitude is shown in color using the rainbow palette, the release events are marked by horizontal lines, and the red curves show the electron cyclotron frequency and its first five harmonics. This release was done at high pitch angles starting at 94.8° when the valve was opened and ending at 113° when it was closed, as marked toward the bottom of the plot. The top panel shows the on/off history of the Hall plasma source (which was always in the no-discharge mode) and is not important for the case of neutral gas releases.

The following observations can be noted in the HF wideband plot:

1. There is narrowband activity (appearing as a blue band with shades of green) centered at a frequency of about 3.7 MHz that starts at the time the valve is on (within the temporal resolution of the instrument) and lasts until the valve is turned off, after which time it decays in bandwidth and amplitude. (The apparent delay in the appearance of this activity with respect to the "valve on" event is beyond the temporal resolution of the HF wideband data. In other words, within the time resolution of the instrument, the beginning of the wave activity and the "valve on" event coincide.)
2. There is more broadband activity (appearing as a mostly green band with shades of blue) extending from a frequency of about 8 MHz to at least 10 MHz that has the same features as the activity described above except that it ends more abruptly when the valve is turned off.
3. Both of the above described bands are flat with respect to time and do not reflect the changes in the magnetic field strength reflected by the electron cyclotron harmonics shown on the same plot.
4. All other features are either natural ionospheric phenomena or wave activity that is not affected by the release.

We cannot presently offer an explanation for the exact nature of these observed wave activities. Since their frequencies do not reflect the substantial changes in the magnetic field and densities occurring during the time interval the data were recorded, they may not be directly related to natural plasma frequencies. Nonetheless, the fact remains that their appearance and their observed features correlate well with gas release events.

Another example of the HF wideband data for a high–pitch angle release is shown in Plate 2. The release was made during orbit number 490 with orbital parameters shown in Table 1.

The same comments made for the wideband data of the release of orbit 419 apply for the activity in the plot of Plate 2 with the additional observation that there is a clear enhancement of the wideband noise across the entire spectrum starting from the time the injection system is turned on and ending at the time when all injection subsystems are turned off.

Two examples of low–pitch angle releases are shown in Plates 3 and 4 (for orbits 426 and 496). The corresponding orbital data are also shown in Table 1.

In contrast to the high–pitch angle releases discussed above, these plots show no wave activity that can be correlated with any of the events associated with the neutral gas release.

It is important to note that although the above described effects correlate well with the pitch angle for all the cases studied, it is not clear whether this correlation is fortuitous, since other conditions, such as orbital position, solar illumination, and associated plasma environment, which have correlations with the pitch angle, may be the true controlling parameters for the appearance of the above mentioned emission.

Since, as already noted above, all investigated gas releases with large pitch angles were done in sunlight, and all injections at small pitch angles occurred in darkness, it is possible that the presence of the solar flux and not the magnitude of the pitch angle is the controlling parameter for the effects described above. In such a case, the role of the solar flux in affecting HF wideband activity through intermediary effects such as plasma enhancement due to photoionization may be worthy of investigation. Since the solar flux does not vary much during the time of the release and since the release mass flow rate is constant, such a mechanism may offer a possible explanation for the constancy of the frequency of the excited bands as a function of time.

Finally, we cannot rule out the role of ground-based broadcasting stations in creating the flat frequency bands observed in the HF spectra. This scenario, however, begs the question of why these bands appear (or are enhanced) only during the releases and not after.

3.2. Plasma Parameters

The measurements of electron temperature along and across the magnetic field, plasma density, plasma potential, and satellite potential made by the KM-10 instrument are shown in Figure 1. Generally, the background plasma is characterized by an electron temperature measured at 2500 K (0.2 eV) and a plasma density of 10^5 cm^{-3}.

The local plasma density (Figure 1a) and spacecraft potential (Figure 1e) do not seem to be affected by the neutral gas release. While the electron temperature measurement in the z direction was marred by a telemetry error, the other two components indicate that there is a peak in the temperature that does coincide with the gas injection. This may be interpreted as evidence of the heating resulting from the interaction described in the next section.

4. Theoretical Models and Calculations

The neutral xenon gas is injected from APEX by a Hall thruster operating in a no-discharge mode at a mass flow rate of 5 mg s^{-1}, which corresponds to $dN_{\mathrm{Xe}}/dt \approx 2 \times 10^{19}$ atoms s^{-1}. The average exhaust speed v is about 1–2 v_T, where v_T is the thermal speed of Xe in the tank. We expect $v_T \leq 10^4$ cm s^{-1}. Consequently, a cloud of neutral gas, driven with a speed of 5–8 km s^{-1} (orbital velocity) through the background ionospheric plasma, will be formed around the spacecraft. We expect, based on ground testing in vacuum, that the cloud will form a spherical cone with a solid angle 60°. The xenon gas density in the spherical cone at a distance r is assumed to be homogeneous across the cross section and can be estimated as

$$n_{xe} = \frac{dN_{\mathrm{Xe}}}{dt}\frac{1}{2\pi r^2 v_T} = \frac{3 \times 10^{14}}{r^2}. \qquad (2)$$

Here $dN_{\mathrm{Xe}}/dt = 2 \times 10^{19}$ atoms s^{-1}, and $v = v_T \leq 10^4$ cm s^{-1}. As an example, at $r = 100$ m, the gas density is $n_{xe} = 3 \times 10^6$ cm^{-3}, and at $r = 1000$ m, $n_{xe} = 3 \times 10^4$ cm^{-3}.

If some of these Xe atoms are ionized, the interaction of these "seed" charged particles with the ambient plasma may lead to the formation of an ion beam and could ignite the process of turbulence-enhanced ionization [*Papadopoulos*,

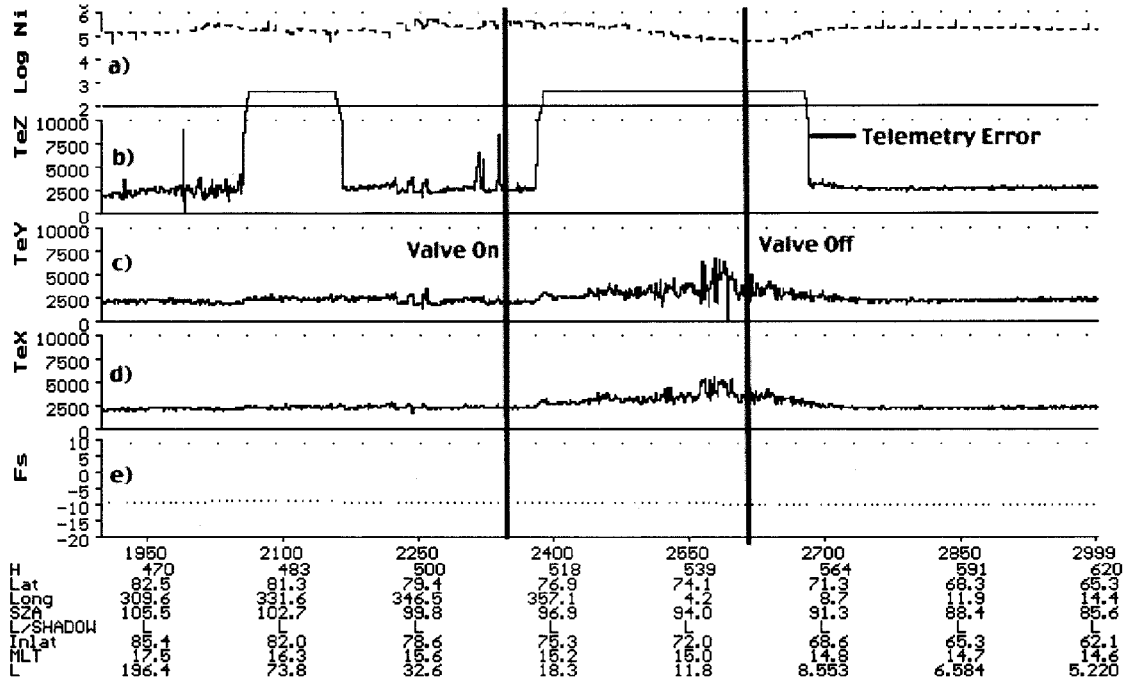

Figure 1. Plasma measurements made with the KM-10 instruments: (a) plasma density; (b)–(d) electron temperature in three directions; and (e) spacecraft potential.

1985; *Okuda and Choueiri*, 1994]. There are several possible processes that may result in the creation of such ion seed from injected xenon neutrals: (1) charge-exchange collisions with ambient oxygen ions, (2) photoionization, and (3) impact ionization by ambient electrons. We start by considering each of these three processes and then considering another process that can lead to ion beam formation through the scattering of ambient oxygen ions. We subsequently estimate the level of electron heating resulting from the formations of such ion beams and end with an estimate of the ionization yield resulting from impact of injected Xe atoms by suprathermal electrons.

4.1. Xe Ion Seed Creation Through Charge-Exchange Collisions and Photoionization

Inelastic charge-exchange collisions of Xe atoms with O^+ ions have a cross section $\sigma_{ch} \approx 2 \times 10^{-15}$ cm^2, that is, less than the cross section for elastic collisions. The local rate of production of Xe ions by charge exchange collisions can be estimated according to the formula

$$\frac{dn_{\mathrm{Xe}^+}}{dt} = \langle \sigma_{ch} n_i v \rangle n_{\mathrm{Xe}}.$$

Considering that the number of injected atoms grows linearly in time, we find, after integration over time and volume, the total number of Xe ions formed in time t due to charge-exchange collisions with ambient plasma ions,

$$\bar{N}_{\mathrm{Xe}^+} = t \int \langle \sigma_{ch} n_i v \rangle n_{\mathrm{Xe}}\, dV = \langle \sigma_{ch} n_i v \rangle t \int^{r/v_T} \frac{dN_{\mathrm{Xe}}}{dt} \frac{d^3 r}{2\pi r^2 v_T}$$

$$\approx \langle \sigma_{ch} n_i v \rangle t \frac{dN_{\mathrm{Xe}}}{dt} \frac{r}{2\pi v_T} \sim \langle \sigma_{ch} n_i v \rangle \frac{dN_{\mathrm{Xe}}}{dt} \frac{t^2}{2\pi}$$

$$\approx 5 \times 10^{14} t^2,$$

where $v \approx v_{sc} \approx 8 \times 10^5$ cm s^{-1} and we have used the measured ion density, $n_i \approx 10^5$ cm^{-3}.

As for photoionization, folding the xenon photoionization cross section with the solar spectral flux allows the calculation of a time constant for Xe ionization in sunlight of 2.2×10^5 s [*Wescott et al.*, 1992]. This yields the following estimate for the total number of photoionized Xe ions at a time t:

$$2 \times 10^{19} t(1 - \exp(-t/2.2 \times 10^5)),$$

which, on timescales of the APEX releases (100–1000 s), is more than a factor of 5 smaller than ion production through charge exchange.

It is difficult to observe these newly born ions with the diagnostics on APEX. First, the Larmor radius for Xe ions is too large, $r_L \geq 500$ m, and second, owing to $\mathbf{E} \times \mathbf{B}$ drift and relative initial velocity, Xe ions do not generally reach the location of the plasma diagnostics.

4.2. Xe Ion Seed Creation Through Impact by Plasma Electrons

The estimation of the number of Xe ions produced from impact by plasma electrons can be done just as it was done in the previous section. Here, however, it is necessary to take into account an essential difference, namely, that at the electron temperature of the ambient plasma the number of electrons with energy exceeding the ionization potential is small. Therefore the effective frequency of ionization is

$$\langle \sigma_{e\mathrm{ion}} n_e v \rangle \approx 10^{-16} n_e v_{Te} \exp(-eU_i/Te),$$

where $U_i = 12.3$ eV is the ionization potential for xenon. The local rate of Xe seed ion production can thus be estimated according to

$$\frac{dn_{\mathrm{Xe}^+}}{dt} = \langle \sigma_{e\mathrm{ion}} n_e v \rangle n_{\mathrm{Xe}} \approx 10^{-16} n_e v_{Te} \exp(-eU_i/Te) n_{\mathrm{Xe}}.$$

Now we can evaluate the total rate of Xe ion production by electron impact as

$$\bar{N}_{Xe^+} = t \int \langle \sigma_{eion} n_e v \rangle n_{Xe}\, dV \approx \langle \sigma_{eion} n_e v \rangle t \frac{dN_{Xe}}{dt} \frac{r}{v_T}$$

$$\approx 10^{-16} n_e v_{Te} \exp(-eU_i/Te) \frac{dN_{Xe}}{dt} t^2. \quad (3)$$

Even for an electron temperature as high as 1 eV, the above expression, with $n_e \approx 10^5$ cm^{-3}, gives a Xe ion production of $4 \times 10^9 t^2$, which is 5 orders of magnitude less than ion production due to charge exchange. Using the measured value for the electron temperature, $T_e \approx 0.2$ eV, ion production by thermal electron impact is totally negligible.

The consequences of the creation of Xe ion seeds in the ambient plasma will be discussed below. There is, however, another process, not considered above, which may be an effective source of plasma perturbation and may result in the generation of waves, heating of ambient plasma electrons, and creation of ion seeds. This process is the scattering of ambient plasma ions by elastic collisions with the injected neutral gas. It is considered in the next section.

4.3. Scattering of Ambient Plasma Ions by Elastic Collisions With the Injected Neutral Gas

In the vicinity of the gas injector the density of Xe gas is large, and collisions of Xe atoms with ambient plasma ions can be important. We can estimate the distance r_c from the injector that corresponds to the mean free path of ions colliding with the neutral gas, $\lambda = 1/\sigma n_{xe}$. We find that for a total elastic cross section of $\sigma \approx 10^{-14}$ cm^2, practically all the relative flow of ionospheric plasma through the beginning of the injected Xe cloud will be stopped (or reflected) at a distance of only a few centimeters.

These elastic collisions can have an influence up to distances of a few tens of centimeters. The probability for ionospheric ions to be scattered by the Xe cloud on their path dl is $\sim dl/\lambda$. A flow of ionospheric ions $\sim \langle n_i v \rangle$ passing through a differential volume length dl and differential area dS in the Xe cloud loses

$$d\bar{N}_i = \langle n_i v \rangle dS \frac{dl}{\lambda} = \langle n_i v \rangle \sigma n_{xe} dS\, dl$$

particles per unit time. The total number of the reflected ionospheric ions per unit time is given by the expression

$$\bar{N}_i = \langle n_i v \rangle \int \sigma n_{xe} dS\, dl = \langle n_i v \rangle \sigma \int n_{xe}\, dV = \langle n_i v \rangle \sigma N_{Xe},$$

where N_{Xe} is the total number of injected Xe atoms. So for parameters typical of the APEX releases, $n_i \approx 10^5$ cm^{-3}, $v \approx v_{sc} \approx 8 \times 10^5$ cm s^{-1}, after t seconds the total number of reflected O^+ is

$$\bar{N}_i = \langle n_i v \rangle \sigma \frac{dN_{Xe}}{dt} t \approx 10^{16} t. \quad (4)$$

The change in kinetic energy due to collisions between oxygen ions and Xe atoms is small due to the large difference between the O^+ and Xe atomic masses. Therefore, to a first approximation, the distribution of the reflected ions may be considered to be isotropic in the coordinate system of the Xe cloud (spacecraft). The ionospheric ions scattered by the neutral cloud are magnetized and continue their $\mathbf{E} \times \mathbf{B}$ drift in the cloud's coordinate system together with the main plasma, but in the coordinate system of the ionospheric plasma, on distances less than their Larmor radii, the reflected ions form a warm ion beam with drift velocity $\sim v_{sc}$ and velocity spread $\sim (1/2\text{–}1/3) v_{sc}$.

Therefore a portion of the flow of ionospheric ions is captured by the neutral Xe cloud. The density of ionospheric oxygen ions can thus increase, and this "plugging" effect can be observable. The main effect of these scattering collisions, however, is the formation of an unstable (beam-like) ion velocity distribution function and, as a result, generation of lower hybrid fluctuations in the plasma. The formed ion beam is strongly inhomogeneous in space. We can estimate the beam density (which is the basic parameter that controls the conditions for instability) if we assume that on a distance R the main contribution to the density of the beam is made by ions reflected at $r < R$ and $t \approx R/v_T$. Thus

$$\frac{n_b}{n_i} = \frac{\bar{N}i}{n_i v_{sc} R^2} = \frac{\langle n_i v \rangle}{n_i v_{sc} R^2} \sigma \frac{dN_{Xe}}{dt} \frac{R}{v_T} \approx \frac{\sigma}{v_T R} \frac{dN_{Xe}}{dt} = \frac{20}{R}.$$

At $R \leq 10^4$ cm we get $n_b/n_i \approx 2 \times 10^{-3}$.

4.4. Electron Heating

The acceleration or heating of electrons by waves produced by the ion-ion instability is usually considered as an essential part in a chain of events resulting in the "anomalous" (or turbulence-driven) ionization in a collisionless plasma. An estimation of the typical mean free path for elastic collisions between ionospheric electrons and the injected Xe ions ($\sigma_{e\text{–}Xe} \sim 0.3\text{–}1 \times 10^{-15}$ cm^2) is (see equation (2))

$$\lambda_{e\text{–}Xe} \approx \frac{1}{n_{Xe} \sigma_{e\text{–}Xe}} \approx (3 - 11) r^2,$$

(here r is, again, the distance from the injector in centimeters) and shows that the elastic e–Xe collisions are important only in the immediate vicinity of the source.

A few centimeters from the source, electron collisions are too rare to change their dynamics or distribution. According to the previous consideration, the density of plasma ions, scattered by Xe atoms, is rather high in the vicinity of the source, and in this region the ion-sound-type fluctuations can arise, resulting in the strong heating of electrons (and possibly electron trapping in wave potential). The energy of the accelerated electrons can be estimated, assuming that the resulting ion-ion instability saturates by ion trapping in a potential well φ_{trap}. In this case an electron receives additional energy $\varepsilon \sim e\varphi_{trap} = m_i v dv = 3\text{–}5$ eV, where dv is the difference in the velocities of the ion beam and the wave. We see that it is impossible to accelerate electrons to energy levels higher than the ionization potential of Xe. Such an acceleration can only be possible as a result of a resonant interaction with waves over a much greater length and inside a much larger volume.

Thus, in the vicinity of the injector, the reflected ions form a bump-on-tail distribution, and, in this case, an ion-ion instability develops if the relative velocity V_b between the beam ions and the ambient ions considerably exceeds the thermal velocity of the latter. The ion-sound instability is suppressed in the ionosphere because $T_e \approx T_i$, and under such circumstances the dominant instability produces lower hybrid fluctuations which have a resonant interaction with the ion beam $kV_b \approx$

$-k_\perp|V_b| \approx \omega_{lh} \approx \omega = \omega_c(k_z/k)$, where ω_{lh} and ω_c are the lower hybrid and electron cyclotron frequencies. For such an interaction we typically have $\omega \ll \omega_c$ and the parallel wave vector k_z is less than that perpendicular to the magnetic field, $k_\perp$. Since this is a resonant interaction with a characteristic frequency near the lower hybrid frequency of oxygen, $f_{lh} \approx 5$ kHz, we can estimate the typical wavelength as $\lambda = V_b/f_{lh}$ and find it to be of the order of a meter. Therefore we can assume that the wavelength of unstable waves is generally contained within the cloud of ions and calculate a local growth rate of the ion beam instability following *Mikhailovskii* [1974],

$$\gamma_b = \omega \frac{\omega_{pi}^2}{1 + (\omega_p/\omega_c)^2} \left(\frac{1}{k\Delta V_b}\right)^2 \left(\frac{n_b}{n_i}\right) \sim \omega \left(\frac{n_b}{n_i}\right) \geq 10^2,$$

where ω_{pe} is the Langmuir frequency and ΔV_b, the velocity dispersion in the beam, is in our case $\sim 1/2V_b$.

The threshold of the ion-ion instability is determined by the time for which the waves leave the volume in which the interaction with the beam occurs. This factor can be described by the introduction of an effective damping rate $\nu = V_{gz}/R$, where V_{gz} is the group velocity of waves $V_{gz} = \partial\omega/\partial k_z = \omega/k_z$. The necessary condition for the instability $\gamma_b \geq \nu$ is satisfied at $k_z R \geq n_i/n_b \approx 10^3$.

If the beam velocity is over the threshold, the instability saturates by electron heating from quasi-linear resonant interaction with lower hybrid waves. The equilibrium condition is achieved through a balance between the growth rate and attenuation of waves, described by

$$(\gamma_b + \gamma_e) W_k = 0,$$

where W_k is the wave energy density, and γ_e is the Landau damping due to resonance with magnetized electrons ($\omega = k_z v_{ez}$) and is given by the following expression:

$$\gamma_e = \omega \frac{\omega_{pe}^2}{k^2(1 + (\omega_{pe}/\omega_c)^2)} \left.\frac{\partial F_e}{\partial v_{ez}}\right|_{v_z k_z = \omega}.$$

We can now determine the distribution of electrons accelerated by the wave as a result of the development of the ion-beam instability [see *Lizunov et al*., 1995] with the help of the following equation:

$$\frac{\partial F_e}{\partial v_{ez}} = -\frac{\gamma_b}{\omega} \frac{k_*^2[1 + (\omega_{pe}/\omega_e)^2]}{\omega_{pe}^2} \approx -\frac{m_e}{m_i} \frac{1}{\Delta V^2} \frac{N_p}{N_{\mathrm{Xe}}}. \quad (5)$$

The solution of the above equation gives the universal distribution of accelerated electrons

$$F_e(v_z) = 2 \frac{n_{st}}{n_0} \frac{(v_{\max} - v_z)}{v_{\max}^2}$$

with

$$\frac{n_{st}}{n_0} = \frac{m_e}{m_i} \frac{v_{\max}^2}{\Delta V^2} \frac{N_p}{2N_{\mathrm{Xe}}},$$

where the subscript *st* denotes suprathermal electrons. The maximum velocity to which the waves can accelerate electrons is given by

$$v_{\max}^2 = D_{zz}\tau = D_{zz}L_\parallel/v_{\max}, \quad (6)$$

where

$$D_{zz} = \omega_{pe}^2 \int \left(\frac{k_z}{k_\perp}\right)^2 \frac{E_k^2}{4\pi n m_e} \delta(\omega - k_z v_{ez})\, dk_z\, d\pi k_\perp^2$$

is the coefficient of electron diffusion in velocity space. Further, we use the estimation

$$D_{zz} = v_{Te}^2 \omega_{pe}^2 \frac{W_k}{nT_e} \frac{k_z^2}{v_z k_\perp^2} = v_{Te}^2 \omega_{pe}^2 \frac{W_k}{nT_e} \left(\frac{\omega}{\omega_e}\right)^2 \frac{k}{\omega},$$

where $W_k = \int (E_k^2/4\pi)\, d\pi k_\perp^2$ is the distribution of energy along the streamer $k_\perp = k_\perp(k_z)$. Taking into account the resonance condition, $\omega/k \approx V_b$, we can estimate

$$D_{zz} = \omega_* v_{Te}^2 \frac{\omega_{pe}^2}{2\omega_e^2} \frac{W}{nT_e},$$

where $W = \int W_k\, dk_z$ and ω_* is the frequency corresponding to the peak in the spectrum. Then from (6),

$$\frac{v_{\max}^3}{v_{Te}^3} \approx \frac{\omega_*}{\omega_e} \frac{L_\parallel}{\rho_e} \frac{\omega_{pe}^2}{\omega_e^2} \frac{W}{nT_e}.$$

Unfortunately, quasi-linear theory is not able to determine W/nT_e and ω_* with reasonable accuracy. To get to the possibility of accelerating electrons to energy exceeding the ionization potential ($v_{\max}^2/v_{Te}^2 \geq 30$), the following condition must be reached (at $\omega_{pe}^2/\omega_e^2 = 10$, $\omega_* \approx 10^{-2}\omega_e$):

$$\frac{L_\parallel}{\rho_e} \frac{W}{nT_e} \geq 3 \times 10^3.$$

This condition is rather difficult but possible to satisfy at realistic conditions $W/nT_e = 3 \times 10^{-2}$ and $L_\parallel = 10^5 \rho_e$.

4.5. Ionization of Xe by Suprathermal Electrons

The suprathermal electrons, created by the lower hybrid turbulence, yield further ionization of the injected Xe neutrals and sustain a CIV-type process as in the numerical simulations of *Okuda and Choueiri* [1994]. The ionization rate can be estimated with the help of the calculated electron distribution, as we did for the case of ionization by electron impact (see equation (3)):

$$\frac{dN_{\mathrm{Xe}^+}}{dt} = \int \sigma_{e\mathrm{ion}}(v) F_e(v)\, dv \int n_{\mathrm{Xe}}\, dV \approx \langle \sigma_{e\mathrm{ion}} n_e v \rangle N_{\mathrm{Xe}},$$

$$\frac{1}{t_{\mathrm{ion}}} = \frac{d\, \log N_{\mathrm{Xe}^+}}{dt} \sim \frac{1}{3} \sigma_{e\mathrm{ion}}(v_{\max}) n_{st} v_{\max} \approx 6 \times 10^{-16} n_e \cdot \left(\frac{m_e}{m_i}\right) \frac{v_{\max}^3}{\Delta V^2} \frac{N_p}{6N_{\mathrm{Xe}}} \approx 10^{-16} v_{\max} n_e \frac{m_e v_{\max}^2}{m_i \Delta V^2} \frac{N_p}{N_{\mathrm{Xe}}} \approx 10^{-5}.$$

Here $m_e v_{\max}^2/m_i \Delta V^2 \approx 0.3 - 1$, $N_p/N_{\mathrm{Xe}} \approx 10^{-2}$, $v_{\max} = \sqrt{30}\, v_{Te} \approx 10^8$ cm s^{-1} (at $T_e \approx 0.2$ eV), and the ambient density $n_e \approx 10^5$ cm^{-3}. Therefore on the timescale of the neutral Xe injection from APEX, ~1000 s, less than 1% of the injected neutrals will be ionized. This predicted low ionization yield is a possible explanation for the lack of detected enhancement in plasma density during the APEX releases described in the previous sections.

5. Conclusions

From the above experimental and theoretical studies we conclude the following:

1. The xenon gas releases conducted from the APEX satellite resulted in an enhancement of HF wave activity over a broad band whenever the injection was done at high pitch angles to the local geomagnetic field and in sunlight.

2. No changes of plasma density were detected for any of the releases.

3. Electron temperature measurements indicate electron energy enhancements during the releases.

4. In spite of the small quantity of injected neutral Xe, charge-exchange collisions and scattering of ambient plasma ions by elastic collisions with the injected neutral gas were shown theoretically to produce a sufficient number of energetic seed ions, both newly born Xe ions and scattered ionospheric plasma ions.

5. The conditions favor the formation of an ion-ion instability in the vicinity of the spacecraft. These waves, in the spacecraft coordinate system, have a phase velocity perpendicular to the magnetic field in the range of the velocities of the reflected ions, but their group velocity is directed almost along the magnetic field, so they can reach the spacecraft and can be observed. Unfortunately, the wave detection diagnostics in that band were not operating during the releases. The enhanced broadband activity measured in the HF (0.1–10 mHZ) range may be related to the effect of these turbulent fluctuations.

6. In this quasi-linear interaction the lower hybrid waves accelerate electrons along the magnetic field up to suprathermal energies; these electrons can reach the satellite and be observed. This may explain the recorded enhancement in the average electron energy.

7. The yield of this interaction was calculated, for the parameters of the APEX release, to be less than 1%, resulting in the lack of a detectable change in the recorded plasma density.

Acknowledgments. Part of this work was supported by the U.S. Air Force Office of Scientific Research, Directorate of Aerospace and Materials Sciences.

Janet G. Luhmann thanks Jill A. Marshall and another referee for their assistance in evaluating this paper.

References

Alfvén, H., *On the Origin of the Solar System*, Oxford Univ. Press, New York, 1954.

Biasca, R., Numerical simulation of the critical ionization velocity mechanisms, Ph.D. thesis, Mass. Inst. of Technol., Cambridge, 1992.

Brenning, N., Review of the CIV phenomenon, *Space Sci. Rev*., *59*, 209–314, 1992.

Burch, J., W. Roberts, W. Taylor, N. Kawashima, J. Marshall, S. Moses, T. Neubert, S. Mende, and E. Choueiri, Space experiments with particle accelerators: SEPAC, *Adv. Space Res*., *14*(9), 263–270, 1994.

Choueiri, E., R. Jahn, H. Okuda, V. Oraevsky, V. Dokukin, and V. Volokitin, Anomalous ionization and the MPD thruster: Investigations of the critical ionization velocity (CIV) phenomenon in space, yearly technical report to Air Force Office of Scientific Research, *Contract F49620-93-1-0222*, Electr. Propul. and Plasma Dyn. Lab., Princeton Univ., Princeton, N. J., 1994.

Haerendel, G., Alfvén's critical velocity effect tested in space, *Z. Naturforsch. A*, *37*, 728–735, 1982.

Haerendel, G., M. Kelley, and R. Pfaff, Electric field measurements during the condor critical velocity experiment, *J. Geophys. Res*., *91*, 9939–9946, 1986.

Lizunov, G., V. Oraevsky, and A. Volokitin, Whistler generation by an ion beam limited in the transverse direction, *Plasma Phys. Rep*., *21*, 85–88, 1995.

Marshall, J., J. Burch, E. Choueiri, and N. Kawashima, CIV experiments on ATLAS 1, *Geophys. Res. Lett*., *20*, 499–502, 1993.

Mikhailovskii, A., *Theory of Plasma Instabilities*, Consult. Bur., New York, 1974.

Möbius, E., R. Boswell, A. Piel, and D. Henry, A Spacelab experiment on the critical ionization velocity, *Geophys. Res. Lett*., *6*, 29–31, 1979.

Okuda, H., and E. Choueiri, Numerical simulation of neutral gas release experiments in the ionosphere, *Phys. Plasmas*, *1*, 1669–1675, 1994.

Papadopoulos, K., On the physics of the critical ionization velocity phenomena, in *Advances in Space Plasma Physics*, *Proceedings of the 1985 Plasma Physics College in Trietse, Italy*, pp. 33–58, World Sci., River Edge, N. J., 1985.

Swenson, C., M. Kelley, F. Primdahl, and K. Baker, CRIT II electric, magnetic, and density measurements within an ionizing neutral stream, *Geophys. Res. Lett*., *17*, 2337–2340, 1990.

Swenson, G., S. Mende, R. Meyerott, and R. Rairden, Charge exchange contamination of CRIT-II barium CIV experiment, *Geophys. Res. Lett*., *18*, 401–403, 1991.

Torbert, R., Review of critical velocity experiments in the ionosphere, *Adv. Space Res*., *10*(7), 47–58, 1990.

Wescott, E., H. Stenbaek-Nielsen, and D. Hampton, Xenon critical velocity releases from the ACTIVNY satellite: Discussion of attempted optical observations, *Geophys. Res. Lett*., *19*, 2079–2081, 1992.

V. V. Afonin, Space Research Institute, 117810, 84/32 Profsoyuznaya Str, Moscow, Russia.

E. Y. Choueiri, Electric Propulsion and Plasma Dynamics Laboratory, Applied Physics Group, Princeton University, Princeton, NJ 08544, USA. (choueiri@princeton.edu)

V. S. Dokukin, V. N. Oraevsky, S. A. Pulinets, Y. Y. Ruzhin, and A. S. Volokitin, Institute of Terrestrial Magnetism, Ionosphere and Radio Wave Propagation, Troitsk, Moscow Region, 142092, Russia.

(Received February 9, 2001; revised May 18, 2001;
accepted June 21, 2001.)